LANGMUIR

pubs.acs.org/Langmuir Article

Mixing in Langmuir Monolayers: Perfluorotetradecanoic Acid and a Gemini Surfactant without a Linker

Srikant Kumar Singh, Wei Bu, Pan Sun, and Matthew F. Paige*



Cite This: Langmuir 2023, 39, 16503-16512



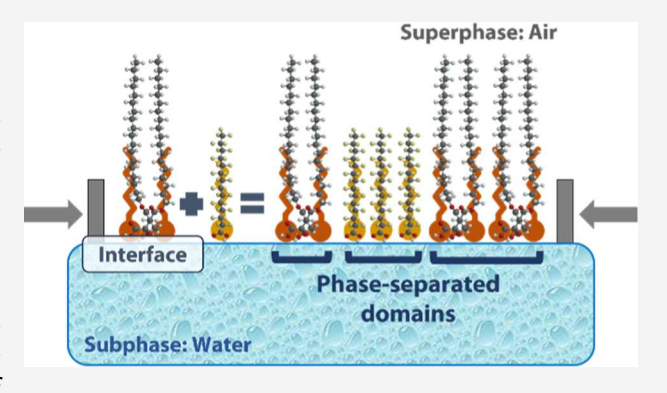
ACCESS

III Metrics & More

Article Recommendations

SI Supporting Information

ABSTRACT: A recently reported anionic gemini surfactant, a member of the so-called "gemini without a linker" family, has recently been reported to form closely packed crystalline monolayers at the air—water interface. In this work, the impact on monolayer properties of the compound, C_{18} -0- C_{18} , that result from its mixing with a benchmark perfluorinated surfactant, perfluorotetradecanoic acid (PF), is explored. The films exhibit nonideal mixing, as determined by surface pressure—area (π -A) isotherms and surface potential measurements, and phase-separation between the two components was observed by the direct visualization of the monolayers, and grazing-incident X-ray diffraction at the air—water interface. The pure and mixed films follow similar trends in the order of C_{18} -0- C_{18} < PF < χ_{PF} = 0.50 mixed films for both their extent of



hysteresis and their stability at the air—water interface. Further, crystallographic data for the mixed film emerge as a simple combination of distinct diffraction patterns characteristic of both the individual components, consistent with the other findings reported here and thus clarify the intermolecular behavior of the binary mixture at the surface.

■ INTRODUCTION

Gemini surfactants, dimeric surfactant molecules with two nominal head groups, are of enormous academic and industrial interest because of their excellent and versatile technical properties. A diverse range of gemini surfactants has been synthesized and reported in the literature (see Sharma et al., for a recent review) and a significant emphasis has been placed on correlating the chemical structure of the linker group that joins the two surfactant head groups with its resulting interfacial behavior, as the linker appears to be of crucial importance in dictating properties of interest (e.g., critical micelle concentration and others). From this perspective, a new class of anionic gemini surfactants, referred to as "gemini surfactants without a spacer group",2 in which the linker length is the minimal possible size (a single covalent bond), is of particular interest. These minimal linker geminis can be viewed as marking the extreme limit in terms of headgroup compactness, thus making them useful test cases for evaluating structure-property relationships in surfactant aggregate

Our research group has recently reported on the physical, chemical properties of monolayers prepared from a minimal spacer gemini surfactant with two carboxylic acid—based head groups and two 18-carbon long alkyl tail chains (C_{18} -0- C_{18} ; Scheme 1) and compared properties of the monolayers the compound forms with several comparator systems, including a closely affiliated gemini with a bulkier linker [Ace(18)-2-Ace(18); two CH₂ groups in linker].³ C_{18} -0- C_{18} is synthetically

accessible through acid-catalyzed coupling of primary alcohols to tetrahydrophthalic anhydride, followed by oxidation to yield the dimeric surfactants in good yield, and similar structures have been reported by others.^{4,5} The key outcome of this study was that the C₁₈-0-C₁₈ monolayers were stable at the air-water interface and shared many similar characteristics with monolayers formed from monomeric fatty acids, including forming highly ordered, crystalline films that exhibited a classic tilted to untilted condensed phase-transition at ambient temperature. Molecular packing density in compressed C₁₈-0-C₁₈ monolayers was found to be approximately double that of typical single-chain fatty acids. This contrasted sharply with monolayers formed from the bulkier spacer group comparator, which were entirely liquid in nature, and the difference was attributed to the ability to pack the inflexible headgroup of minimal spacer gemini more efficiently into films. The formation of a crystalline monolayer in a gemini surfactant system appears to be a rarity in the literature, highlighting the novelty of this system.

Received: August 22, 2023 Revised: October 20, 2023 Accepted: October 23, 2023 Published: November 6, 2023





Scheme 1. Representative Chemical Structures of (A) C₁₈-0-C₁₈ (B) Perfluorotetradecanoic Acid (C) Perfluorooctadecanoic Acid

An ongoing, related topic of investigation with this class of surfactants and affiliated molecules is their miscibility with perfluorinated surfactants in monolayers. Mixed monolayers of hydrogenated and perfluorinated surfactants are frequently phase-separated at the air—water interface, driven in part by the low molecular polarizability of the perfluorocarbon. Immiscibility is further refined by the molecular-level interactions between surfactants that are a function of the detailed chemical structure of the film constituents. This mutual immiscibility can lead to intriguing pattern formation in a variety of mixed films, and the subject matter has been reviewed extensively elsewhere. Work in our group has focused on mixed systems containing simple perfluorinated fatty acids, primarily perfluorotetradecanoic acid [PF; CF₃(CF₂)₁₂CO₂H, Scheme 1].

Mixing properties of C₁₈-0-C₁₈ and perfluorocarbons have been entirely unexplored in the literature, and the minimal linker gemini provides an opportunity to explore the impact of PF on miscibility and film structure with a gemini surfactant that packs efficiently into crystalline monolayers. We have previously reported that binary mixed monolayers of Ace(18)-2-Ace(18) (bulky linker noted above) and PF were immiscible, with weak repulsive interactions between the two components leading to the formation of phase-separated domains at the air-water interface. While the gemini surfactant remained liquid-like in the mixed monolayers, the PF component formed crystalline regions, albeit with a significantly distorted lattice structure in comparison with pure monolayers of PF. Shorter tail-chain variants of the gemini gave similar results, though the mixing thermodynamics were significantly more complicated; shorter hydrocarbon chains likely resulted in weaker cohesion within the phase-separated hydrocarbon region because of weaker dispersion forces between close-packed tail chains.9 The working hypothesis for the current C_{18} -0- C_{18} system is that the monolayer will be phase-separated, akin to the PF-Ace(18)-2-Ace(18) mixed films, with both components exhibiting monolayer crystallinity because of their excellent packing abilities. This is similar to what was observed for a binary mixed monolayer of arachidic acid with PF, 10 which

might reasonably be viewed as a monomer analogue for the mixed gemini-PF system investigated here. The remainder of this work tests this hypothesis and discusses the results in the context of the various comparator systems that are described in the literature.

■ EXPERIMENTAL SECTION

Materials. The synthesis, purification, and characterization of C_{18} -0- C_{18} have been reported elsewhere. PF was purchased from Sigma-Aldrich and used without further purification (purity 96%). Chloroform (>99.8%) and hexanes (>98.5%) were obtained from ThermoFisher Scientific. Tetrahydrofuran (THF; \geq 99.9%) was procured from Millipore Sigma. Stock solutions of C_{18} -0- C_{18} were prepared in chloroform (1 mM), and those of PF were prepared in a 9:1 hexanes/THF mixture. For binary solutions of C_{18} -0- C_{18} and PF, aliquots from the stock solutions were mixed volumetrically to obtain appropriate mixed film compositions. Film compositions are described in terms of the mole fraction of PF (χ_{PF}). All solvents used in the preparation of solutions were obtained from Sigma-Aldrich and were ACS grade or better.

Film Preparation and Characteristics. Langmuir films of C₁₈-0-C₁₈, PF, and their mixtures were prepared on a Langmuir trough (KSV Biolin; KN 2006) filled with ultrapure water (Barnstead, resistivity = 18.2 $M\Omega \cdot cm^{-1}$) subphase. The surface pressure was measured with a Wilhelmy balance and a filter paper plate (1 cm \times 2 cm; Whatman). The trough and the barriers were thoroughly cleaned with pure ethanol and deionized water several times prior to the initial measurements. The water surface was cleaned by suction with an aspirator, and blank runs were performed to ensure a clean surface. The trough (and the barriers) was rinsed with chloroform and wiped with surfactant-free tissue between replicates. Two barriers enabled symmetric (lateral) compression of the film at a rate of 20 mm²·min⁻¹ (approximately 5.0 Å² molecules·min⁻¹), and blank runs were recorded to ensure that the subphase surface was clean. The surfactant solutions (100 μ L) were then spread onto the clean subphase using a Hamilton syringe (100 μ L volume), and the films were compressed after ~15 min (allowing for solvent evaporation and stabilization of the film). Three replicate isotherms were performed for each system to ensure reproducibility, with film areas varying by less than ±1.0 Å²·molecule⁻¹. Surface potential measurements were performed with a vibrating plate probe (KSV surface potential meter, 3000SP, calibrated with a known DC voltage) mounted on the trough.

Monolayer Film Characterization. For micrometer-scale imaging, films at the air—water interface were illuminated by a 658 nm laser using an UltraBAM microscope (KSV Biolin/Accurion) equipped with a camera operating at an acquisition rate of 20 frames $\rm s^{-1}$

Liquid Surface X-ray Measurements. Grazing incidence X-ray diffraction (GIXD) and X-ray reflectivity (XR) measurements were carried out on a liquid surface scattering reflectometer in the 15-ID-C (ChemMatCARS) sector of the Advanced Photon Source (Argonne National Laboratory). For these measurements, monolayer films of pure components and a $\chi_{\rm PF}$ = 0.50 mixture as a representative of the mixed films were prepared on a Langmuir trough with a single movable barrier, and the trough was encased in a sealed chamber mounted on an active vibration isolation table. The chamber was purged with helium, and the oxygen level was kept below 2% during X-ray experiments to minimize X-ray beam scattering and ensure minimal beam-induced damage to the film. A monochromatic X-ray beam with an energy of 10.0 keV was directed onto the subphase surface at an incident angle of ~0.1° upon spreading the appropriate surfactant solution onto the subphase in the trough. Compression experiments were kept consistent with the method described in the preceding section. Diffracted (or reflected) X-rays were collected on a Pilatus 3 200 K X-ray detector (Dectris).

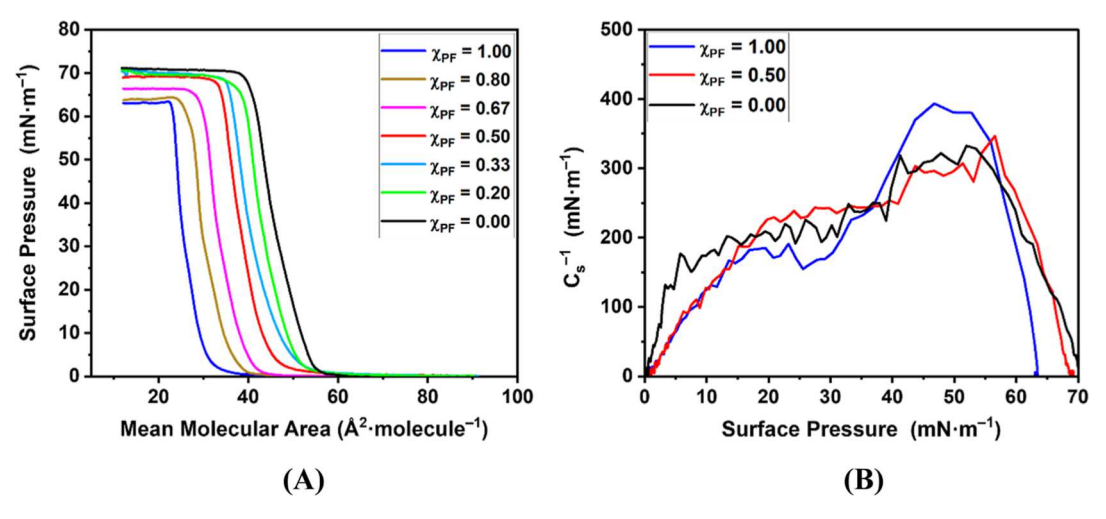


Figure 1. (A) Isotherms and (B) compressibility modulus plots of pure and mixed PF-C₁₈-0-C₁₈ film(s).

RESULTS & DISCUSSIONS

Compression Isotherms. Surface pressure—area $(\pi - A)$ compression isotherms for monolayer films of PF, C_{18} -0- C_{18} , and five PF: C_{18} -0- C_{18} mixtures, representing a total of seven different film compositions, are shown in Figure 1. Key numerical data extracted from the isotherms are summarized in Table 1. To detect phase transitions otherwise not visible in

Table 1. Summary Isotherm Data for the PF- C_{18} -0- C_{18} Monolayer Films^a

$\chi_{ ext{PF}}$	A_0 (Å 2 /molecule)	$\pi_{\rm c}~({\rm mN\cdot m^{-1}})$
1.00	26.9 ± 0.5	63.5 ± 0.9
0.80	32.1 ± 0.6	64.5 ± 0.3
0.67	35.8 ± 0.9	66.2 ± 0.2
0.50	42.0 ± 0.7	68.6 ± 0.1
0.33	44.4 ± 0.6	69.0 ± 0.9
0.20	46.6 ± 0.8	69.1 ± 0.8
0.00 (pure C18-0-C18)	50.8 ± 0.3	70.2 ± 0.8

^aUncertainty ranges are standard deviations determined by measuring a minimum of 3 replicate isotherms.

 π –A isotherms, compressibility modulus plots ($C_s^{-1} = -A(d\pi/dA)_T$ vs π) for the pure components and one representative mixed film composition ($\chi_{PF} = 0.50$) are shown in Figure 1B, with plots for the remaining mixed films included in the Supporting Information (Figure S1). The

Supporting Information also includes a detailed description of the trends observed for these data (Section S1; Supporting Information). Monolayers of the pure components were stable at the air-water interface and gave isotherms and compressibility modulus plots that were consistent with those reported previously. 3,11,12 Each of the isotherms (for pure PF, C_{18} -0- C_{18} , and all mixture films) exhibits a steep rise in surface pressure following the "flat" gaseous phase, with no apparent phase transitions until the collapse of the films. The overall shapes of the isotherms register a large slope, which is characteristic of solid-like monolayer films with low compressibility. Since the individual isotherms appear largely featureless, we will focus on discussing trends observed for the limiting mean molecular areas (A_0) , determined by extrapolating the steeply rising portion of the isotherm to zero surface pressure), and the collapse pressures (π_c ; surface pressure at collapse) of the films.

Isotherms for the mixed $PF:C_{18}$ -0- C_{18} monolayers fell between the isotherms for the pure individual component films. Film collapse pressures and the limiting mean molecular areas depended strongly on film composition (Table 1), with films becoming more expanded as the mole fraction of the gemini surfactant in the mixture increased. This is the expected result of increasing the amount of the surfactant with the bulkier headgroup.

Variation of film collapse pressure as a function of composition has classically been assessed using the 2D phase rule. ¹³ For a film composed of two immiscible components at

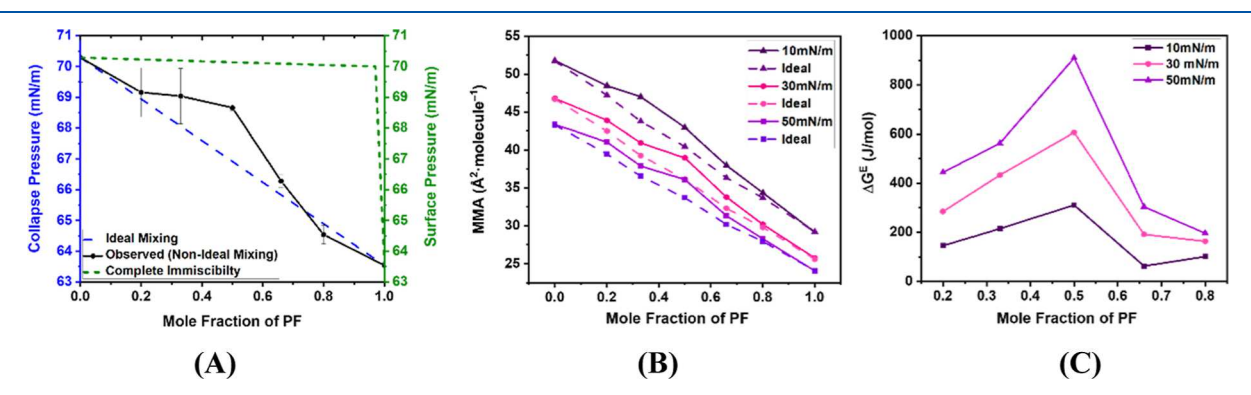


Figure 2. (A) Defay—Crisp plot (B) additivity plots and, (C) plot showing the excess Gibbs free energy of mixing as a function of mole fraction of PF.

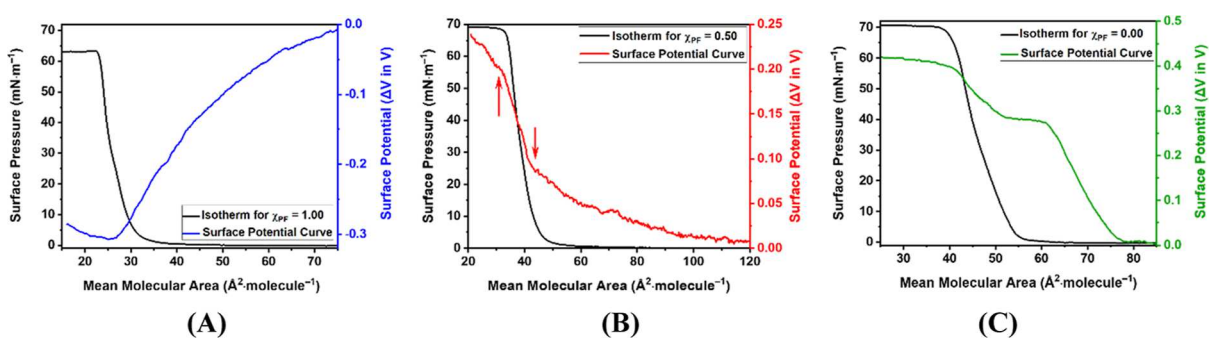


Figure 3. Surface potential curve for (A) PF (B) $\chi_{PF} = 0.50$ mixture (C) C_{18} -0- C_{18}

constant temperature and atmospheric pressure, film collapse pressures will be independent of composition, whereas for a miscible film, the opposite is true. This is shown for the PF-C₁₈-0-C₁₈ mixed systems using a Defay-Crisp diagram, film collapse pressure versus film composition, in Figure 2A; the diagram includes the expected results for both ideal mixing and perfect immiscibility (dashed lines) as per Rose et al. ¹⁴ As seen in Figure 2A, the collapse pressure trends alone indicate nonideal mixing. However, this should be treated with caution, as the rule is limited by the somewhat questionable application of equilibrium thermodynamics to metastable monolayers that may not be in a state of true thermodynamic equilibrium when the collapse occurs. The isotherm data are analyzed in more depth below using conventional additivity analysis. However, the trends in collapse pressure for the mixed system also bear some additional scrutiny, and we report on this before returning to an additivity analysis.

Closer inspection of the collapse pressures shows values do not increase monotonically as a function of the quantity of C_{18} 0-C₁₈, but rather show modest increases, followed by a regime $\chi_{\rm PF} \lesssim 0.50$ in which the collapse pressures are all very similar to that for pure C₁₈-0-C₁₈. This is an effect that has been reported in a number of mixed monolayer systems that contain two types of surfactants, one which has a comparatively large headgroup cross-sectional area to tail, and the other surfactant which has the opposite. The majority of systems reported to date are those containing a phospholipid (large headgroup area to tail ratio). 15-17 In mixed systems, with a sufficient quantity of the surfactant with a large headgroup, there will be an overall lateral connectivity between surfactants, and the surfactants with smaller headgroups fill the empty sites. This leads to the overall film collapsing at the pressure at (or close to) that of the larger headgroup component. Modeling calculations of this effect using percolation theory estimates the mole fraction of bulky headgroup surfactant at which this effect becomes important at $\chi \approx 0.7$. The trends we observe for the mixed PF-C₁₈-0-C₁₈ system are entirely consistent with this effect; the cross-sectional area of the C_{18} -0- C_{18} headgroup is, of course, very large, and the opposite is true for the PF component, and thus this is precisely the type of system in which the effect is expected. At and above this mole fraction of gemini, the collapse pressures essentially converge to those of pure gemini. We note that the majority of systems reported to date which describe this effect have all involved mixtures of phospholipids with simple fatty acids or alcohols, and observing this effect in a phospholipid-free system suggests that the percolation model is broadly generalizable. As a simple test of this, we have carried out similar isotherm measurements with mixtures of C₁₈-0-C₁₈ with perfluorooctanoic acid (PO,

Scheme 1C). The π -A isotherms (Supporting Information, Figure S2) once again show behavior similar to that of the PF-based system and a similar onset composition value, indicating that the effect is broadly observed and common to this bulky headgroup gemini system.

Returning to the original isotherm data, additivity plots (mixed film area as a function of composition) were generated and are shown in Figure 2B, along with the ideal behavior predicted from the additivity relationship for fully immiscible (or ideally mixed) films given by eq 1^{13}

$$A_{12} = A_1 \chi_1 + A_2 \chi_2 \tag{1}$$

where A_{12} is the area for the binary mixed film, A_n is the area of the film for component n, and χ_n is the mole fraction of component n. Deviations in experimental data from (1) are indicative of either repulsive (in the case of positive deviations) or attractive (in the case of negative deviations) interactions between film components. For almost all surface pressures, additivity plots showed modest positive deviations from ideal mixing, indicating repulsive interactions between the film components and that the mixed films were more expanded than their pure individual components. The largest extent of film expansion was ~2.5 Ų·molecule $^{-1}$ for a $\chi_{\rm PF} = 0.50$ mixed film; the extent of expansion is comparable with what was observed for the mixed PF–Ace(18)-2-Ace(18) monolayer system and, in turn, very different from PF–Ace(12)-2-Ace(12), which showed significant film compaction.

The extent of the repulsive interactions with the films was probed by calculating excess Gibbs free energies of mixing (ΔG^{E}) for the mixed films as a function of surface pressure using eq 2.¹³

$$\Delta G^{E} = \int_{0}^{\pi} [A_{12} - (\chi_{1}A_{1} +_{2} A_{2})]d$$
 (2)

using the same definitions as (1). Figure 2C shows a plot of $\Delta G^{\rm E}$ for each mixed film vs mole fraction of PF. The mixed systems gave positive values of excess Gibbs free energy (films destabilized relative to ideality) for all compositions at the three different surface pressures, with values ranging from 62 to 909.8 J·mol⁻¹ (lowest to highest pressures). As expected because of their similarity to the film expansion values, excess Gibbs free energies were also comparable with the PF–Ace(18)-2-Ace(18) system. This is instructive: it suggests the dominant factor dictating the repulsive interaction in the mixed system is simply the interaction between the perfluorocarbon and hydrocarbon tail chains; switching to the more compact C_{18} -0- C_{18} headgroup caused no substantive difference between films, and again, the fundamental incompatibility of hydrocarbons and perfluorocarbons is the dominant interaction.

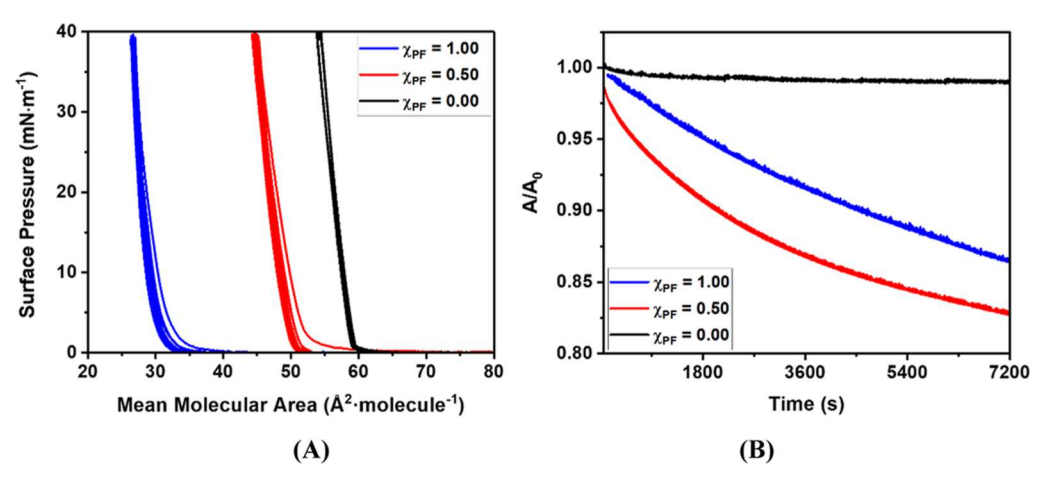


Figure 4. (A) Repeated isocycles for pure and mixed films from $\pi_{max} = 40 \text{ mN} \cdot \text{m}^{-1}$ to $\pi_{min} = 0 \text{ mN} \cdot \text{m}^{-1}$ (B) normalized film area as a function of time curves for pure and $\chi_{PF} = 0.50$ mixed films at $\pi = 30 \text{ mN} \cdot \text{m}^{-1}$.

Surface Potential Measurements. To further elucidate the impact that this interaction between the two film components has upon the structural properties of the film, the surface potential as a function of film area $(\Delta V - A)$ for monolayers of pure components and a representative χ_{PF} = 0.50 mixture was measured, with results shown in Figure 3. For the ensuing discussion, we take the simplest possible interpretation of surface potentials, (e.g., Helmholtz model, with ΔV scaling as the net perpendicular dipole moment of the film). Corresponding isotherms have been included for comparison. We note that perfluorinated fatty acids have molecular dipole moments oriented in the opposite direction relative to hydrogenated fatty acids (e.g., vector pointed away from the headgroup) because of the helical structure of fluorinated chains and the electronegativity of fluorine. 11,19 Thus, for the case of PF, the ΔV values became more negative with film compression, with curves approaching minima immediately prior to monolayer collapse. For pure C_{18} -0- C_{18} films, surface potentials became more positive with film compression. The overall shape of the $\Delta V-A$ plots for the pure components (Figure 3A,C) is consistent with the previous reports.3,11

The surface potentials (ΔV) of the $\chi_{\rm PF}=0.50$ mixed film were positive throughout the compression range and the overall $\Delta V-A$ curve shows two reproducible inflection points (marked with red arrows; Figure 3B). Features in the $\Delta V-A$ curves have previously been used to help identify the presence of phase transitions or other similar changes in the isotherms, and in this case, the inflection points correspond to the steep increase in surface pressure at ~40 Ų·molecule⁻¹ and the onset of film collapse at large and small film areas, respectively. Surface potential measurements follow the same additivity relationships as for compression isotherms, and for an ideal system¹³

$$\Delta V_{12} = \Delta V_1 \chi_1 + \Delta V_2 \chi_2 \tag{3}$$

where ΔV_{12} is the surface potential for the binary mixed film, ΔV_n is the surface potential of the film for component n, and χ_n is the mole fraction of component n. Experimental and calculated values for ΔV_{12} are reported in Table S1 of the Supporting Information. For the three surface pressures studied, modest positive deviations from those in eq 3 were observed, as was the case with the isotherm data. Deviations were on the order of ~ 100 mV larger than ideality. We

interpret this as meaning in the mixed film, the film components are more vertically oriented, (greater net dipole moment perpendicular to air—water interface) than a mixed film in which there is no interaction between components. In this case, the repulsive interaction between the hydrocarbon chains and the fluorinated chains results in a net tendency for the film components to be forced into a more vertical alignment than if there were no interactions. Further, PF, both in pure monolayers and in mixed films, is well-known to be vertically oriented, even in uncompressed films of extremely low surface pressure. $^{20-23}$ This suggests that the primary effect here is upon the C_{18} -0- C_{18} , and it is this component of the film that is being directed into a more vertical orientation by the interactions within the film.

Hysteresis and Film Stability. Monolayer hysteresis and stabilization effects were explored by subjecting films to repeated compression-expansion isotherm cycles. One compression-expansion cycle will be termed an isocycle hereafter. Pure PF, C_{18} -0- C_{18} , and $\chi_{PF} = 0.50$ mixed monolayers all exhibited isocycle hysteresis (Figure 4A). To aid visualization of the observed trends, a plot in Figure 4A has been replotted over a lower x-axis range in Figure S3 (Section S4; Supporting Information). For these experiments, monolayers were compressed up to a target surface pressure of π_{max} = 40 mN·m⁻¹ (e.g., lower than film collapse) and then expanded until reaching a target surface pressure of $\pi_{\min} = 0$ mN·m⁻¹ after allowing 10 s of equilibration time between the compression and expansion segments of an isocycle. For all the three films, each consecutive isocycle gradually shifted toward lower mean molecular areas, suggesting that a slight loss of film material to the subphase was occurring. The largest shift was observed between the first and second isocycle for all films, which is generally the case for most monolayer systems. Qualitatively, the extent of isocycle shift observed for the monolayers was in the order of C_{18} -0- C_{18} < PF < χ_{PF} = 0.50, suggesting that the mixed film was the most prone to loss of surfactant at the air—water interface than either of the two pure mixed films alone. Note, the precise fate of the surfactant, whether it is forced into the subphase, "piles up" to form multilayer regions, or gradually fills interdomain voids, is unclear and not easily resolved from these measurements. Nonetheless, to further assess monolayer stability at the airwater interface, experiments in which the surface pressure was maintained at a constant value, and the change in film area

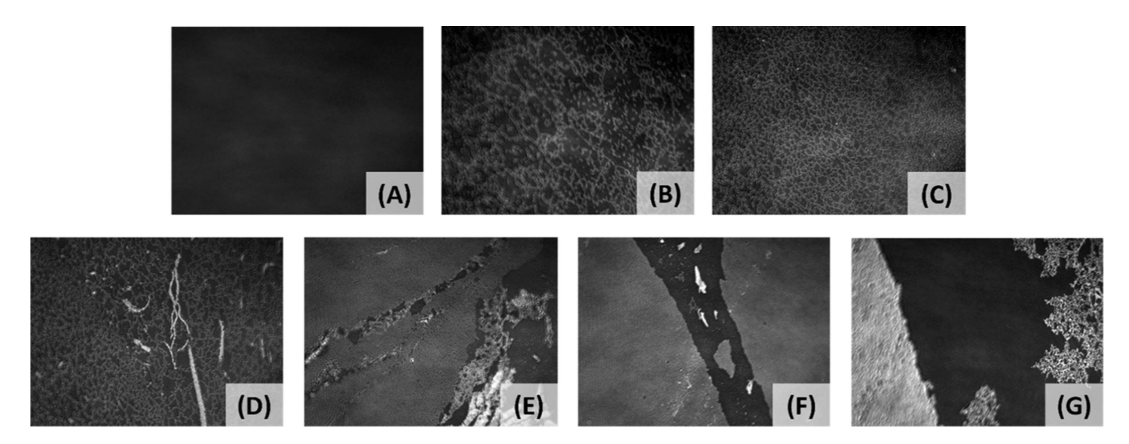


Figure 5. Representative BAM images (696 μ m × 520 μ m) for pure and mixture monolayer films of PF and C₁₈-0-C₁₈ for films compressed to mean molecular area of 55 Å²·molecule⁻¹; (A) pure PF (B) $\chi_{PF} = 0.80$ (C) $\chi_{PF} = 0.67$ (D) $\chi_{PF} = 0.50$ (C) $\chi_{PF} = 0.33$ (F) $\chi_{PF} = 0.20$ (G) pure C₁₈-0-C₁₈. Images were collected at $T = 22 \pm 1$ °C.

required to maintain this surface pressure was measured as a function of time were carried out (similar approaches are described elsewhere; see $^{24-28}$ for example). Figure 4B shows A/A_0 vs time curves for the various

monolayers, where A_0 is the initial mean molecular film area at the beginning of the experiment and A is the time-dependent mean molecular film area. For these experiments, all the films were held at a target surface pressure of $\pi = 30 \text{ mN} \cdot \text{m}^{-1}$ for ~ 2 h. In each case, curves had a downward trajectory, suggesting loss of surfactant from the air-water interface with time. As was the case with the hysteresis studies, each of the monolayers had very different decay curve profiles, both in terms of decay rates and also in terms of the size of the change in film area. We will not attempt a rigorous modeling of decay rates and underlying mechanism(s) of film change as has been carried out for other systems in the literature (see^{24-27} and others), but rather offer a qualitative comparison of the decay profiles for the films. For reference, empirical curve fitting results are shown in the Supporting Information (Section S4). Both of the pure monolayers had film areas that decreased more slowly than that for the mixed film, with the rate, estimated from the initial slope of the decay curve following the order $(C_{18}$ -0- C_{18} < PF < χ_{PF} = 0.50), which is consistent with the trend observed for the area shifts in the isocycle measurements. In terms of magnitude of normalized area change over the duration of the experiment, C₁₈-0-C₁₈ showed the smallest overall change (~1% decrease), followed by pure PF (~13%) and the χ_{PF} = 0.50 mixture (~17%). Clearly, the mixed monolayer is less kinetically stable at the air-water interface than either of the pure components alone, and we can reasonably attribute this to the net repulsive interactions noted in the compression isotherm and surface potential measurements. While speculative, the higher kinetic stability of the pure C₁₈-0-C₁₈ monolayers in comparison with that of the pure PF suggests that the PF component is preferentially forced off the airwater interface in the mixed films, and this remains a topic of future investigation.

Film Morphology. Micron-scale film morphology was assessed using BAM imaging over a range of film compositions and extents of film compression. Figure 5A–G show BAM images for single component control samples and for mixed films at a fixed mean molecular area (55 Å²·molecule⁻¹). Because of the dependence of surface pressure on composition (as per Figure 1A), this means that surface pressures were

slightly different for each film, though for the mixed films, all fell in a pressure range of $\pi \approx 0-5 \text{ mN}\cdot\text{m}^{-1}$. For these measurements, we have chosen to report film structures at a fixed mean molecular area rather than a fixed surface pressure because the isotherms shift as a function of composition, and measuring at fixed surface pressure would mean any differences in film structures observed would be a convolution of film composition and the degree of film compression. However, we also report how film structures vary as a function of surface pressure later in this section. We also note that PF monolayers give negligible image contrast in the BAM (Figure 5A) because of the close match in refractive indices of the perfluorocarbons and the underlying water subphase. Pure C₁₈-0-C₁₈ monolayers yielded reflective (bright) regions in BAM, and thus in images shown below, the bright regions indicate the presence of the hydrocarbon component, while dark regions are either PF or are devoid of surfactant.

For mixed films with a higher mole fraction of PF than C₁₈-0-C₁₈, film morphology consisted of heterogeneous, mesh-like structures (Figure 5B,C). The interior low-reflectivity (dark) regions (the "holes" within the mesh) were generally larger in size for the $\chi_{\rm PF}$ = 0.80 PF-C₁₈-0-C₁₈ mixture than the $\chi_{\rm PF}$ = 0.67 mixture under comparable compression conditions, indicating that a large proportion of these regions is occupied by PF. This indicates that the mixed film is phase-separated, as was seen for the affiliated Ace(18)-2-Ace(18) system we have reported previously.¹² For the $\chi_{PF} = 0.50$ mixture at a similar extent of compression, the mesh structure was still present but contained occasional highly reflective strands, indicating that localized agglomerates of C₁₈-0-C₁₈ were present. All subsequent images for mixed films in which the content of the gemini surfactant was greater than the PF had the same three levels of reflectivity: the dark, PF enriched regions, the interconnected mesh-like structures trapping the darker regions within, and the bright patches and strands enriched in C_{18} -0- C_{18} . For pure C_{18} -0- C_{18} films (Figure 5G), apart from the dark background region ascribed to regions of the film that were devoid of surfactant, the films consisted of highly reflective islands that suggested formation of gemini surfactant deposits.

To assess the dependence of mixed monolayer morphology as a function of film compression, a $\chi_{PF} = 0.33$ monolayer was imaged at a series of different surface pressures. One complication of imaging mixed films over a wide range of

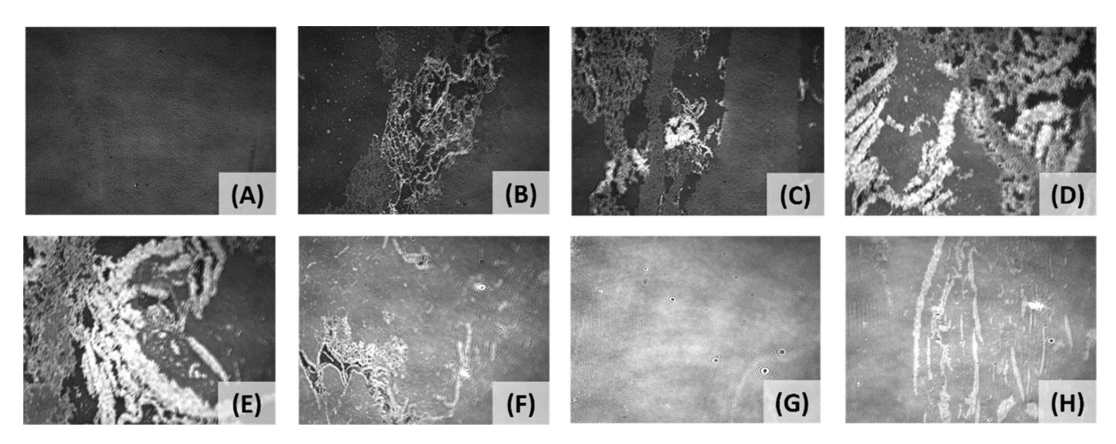


Figure 6. Representative BAM images (696 μ m × 520 μ m) for (A) water only control sample and $\chi_{PF} = 0.33$ mixed monolayer films as a function of surface pressure. Mixed films were measured at surface pressures of: (B) 0–1 (C) 0–2 (D) 2–5 (E) 5–10 (F) 10–15 mN·m⁻¹ (G) from 15 mN·m⁻¹ until film collapse (H) at film collapse.

surface pressures is that film structures can be too compressed to be spatially resolved at higher pressures. For the mixed systems, it was found, empirically, that the composition χ_{PF} = 0.33 was the most well-suited to observe all features of interest, and thus, this composition was studied in detail. Other compositions gave similar structures though at slightly different surface pressures, as expected. Representative images are shown in Figure 6. We note that the overall reflectivity of pure C₁₈-0-C₁₈ films was always higher than that of the mixed films under corresponding conditions, as expected because the total amount of reflective material in the field of view will be larger for pure films than for those that contain PF; this difference is shown in Figure S5 in the Supporting Information for the two films close to their collapse pressure. Initially for the mixed films, at minimal surface pressures, mesh-like structures of varying sizes appear over the darker subphase. As described in Figure 5, we ascribe this to the formation of a network of C_{18} 0-C₁₈ with regions in between occupied by the PF or bare subphase. With further compression, strands and other highly reflective structures are observed, which we interpret as the formation of aggregates of closely packed C₁₈-0-C₁₈. The low reflectivity regions can still be discerned as the film is further compressed until it reaches close to the film collapse (Figure 6H), where presumably surface features (phase-separated regions) are too close together to be spatially resolved. Phase separated structures lack the well-defined domain morphology that has been observed at both the air-water and solid-air interfaces in simple mixed fatty acid-PF systems.7 It is increasingly clear that the chemical structure requirements for the mixed surfactant systems to produce these types of polygonal domains are quite strict and that gemini surfactants used here do not meet this requirement despite their ability to phase separate with PF.

GIXD and X-ray Reflectivity Analyses. Further evidence of immiscibility in the mixed films can be obtained from X-ray scattering measurements at the air—water interface. Both GIXD and XR measurements were completed. XR experiments at various surface pressures were used to assess overall film thickness and to model the electron density profile across the interface, with results reported in Section S6 (Supporting Information). While film thickness and electron density profiles met general expectations for monolayers, simple two-slab modeling did not provide additional insight into possible phase separation, and while more sophisticated models may be explored in the future, GIXD measurements were the primary

focus of this work. Figure 7A–F show GIXD patterns for pure PF, pure C_{18} -0- C_{18} and $\chi_{PF}=0.50$ mixed monolayers at two representative surface pressures of $\pi=10$, and 30 mN·m⁻¹ with crystallographic data for all of the different films and conditions tabulated in the Supporting Information (Section S7). Model perfluorinated amphiphiles like PF exhibit a single diffraction maximum at $q_{xy}\approx 1.24$ Å⁻¹ and pack into crystalline, highly ordered monolayers at the air—water interface, even at very low surface pressures. In line with the previous observations, Figure 7A,B shows a single, sharp Bragg peak positioned at $q_{xy}=1.26\pm0.01$ Å⁻¹ at both surface pressures studied, consistent with the reports cited above. The zero tilt angle for the Bragg rods indicates a normal orientation of PF molecules with respect to the subphase surface.

 C_{18} -0- C_{18} also formed diffracting films and is one of the very few documented examples of a gemini surfactant that forms crystalline monolayer films at the air—water interface.³ At $\pi \approx 10~\text{mN}\cdot\text{m}^{-1}$, GIXD patterns for C_{18} -0- C_{18} monolayers consisted of two Bragg peaks, the first at $q_{xy} \approx 1.40~\text{Å}^{-1}$ ($q_z = 0.56~\text{Å}^{-1}$) and the second peak at $q_{xy} \approx 1.52~\text{Å}^{-1}$ (with $q_z = 0~\text{Å}^{-1}$), corresponding to a centered rectangular lattice with C_{18} -0- C_{18} alkyl chains tilted in the NN direction. Over the pressure range shown here, there were minimal changes in the measured diffraction pattern but we note that at higher pressures the film undergoes a tilted condensed to untilted condensed phase transition akin to that seen in simple monomeric fatty acid monolayers (phase transition at $\pi \approx 40~\text{mN}\cdot\text{m}^{-1}$ appears as discontinuity in compressibility plot in Figure 1B). $^{24,29-32}$ This corresponds to tilted molecules being forced into a more surface normal orientation and manifests as a shift in the out-of-plane peak to lower q_z values.

For the mixed monolayer at the two surface pressures, three diffraction peaks were observed, corresponding to those expected for both PF and C_{18} -0- C_{18} ; the Bragg peak for PF was centered at around the $q_{xy}\approx 1.26~\text{Å}^{-1}$ position ($q_z=0~\text{Å}^{-1}$) along with the in-plane and out-of-plane peaks ($q_z=0~\text{Å}^{-1}$ and $\approx 0.4~\text{Å}^{-1}$) for the C_{18} -0- C_{18} component (Figure 7A–D). The diffraction pattern for the mixed film was essentially a simple combination of the diffraction for the two component pure films, as expected for a fully phase separated film; similar behavior has been presented as evidence for immiscible monolayer systems and adds further support to the occurrence of phase separation between the two components. We do note that there was a slight difference in the position of

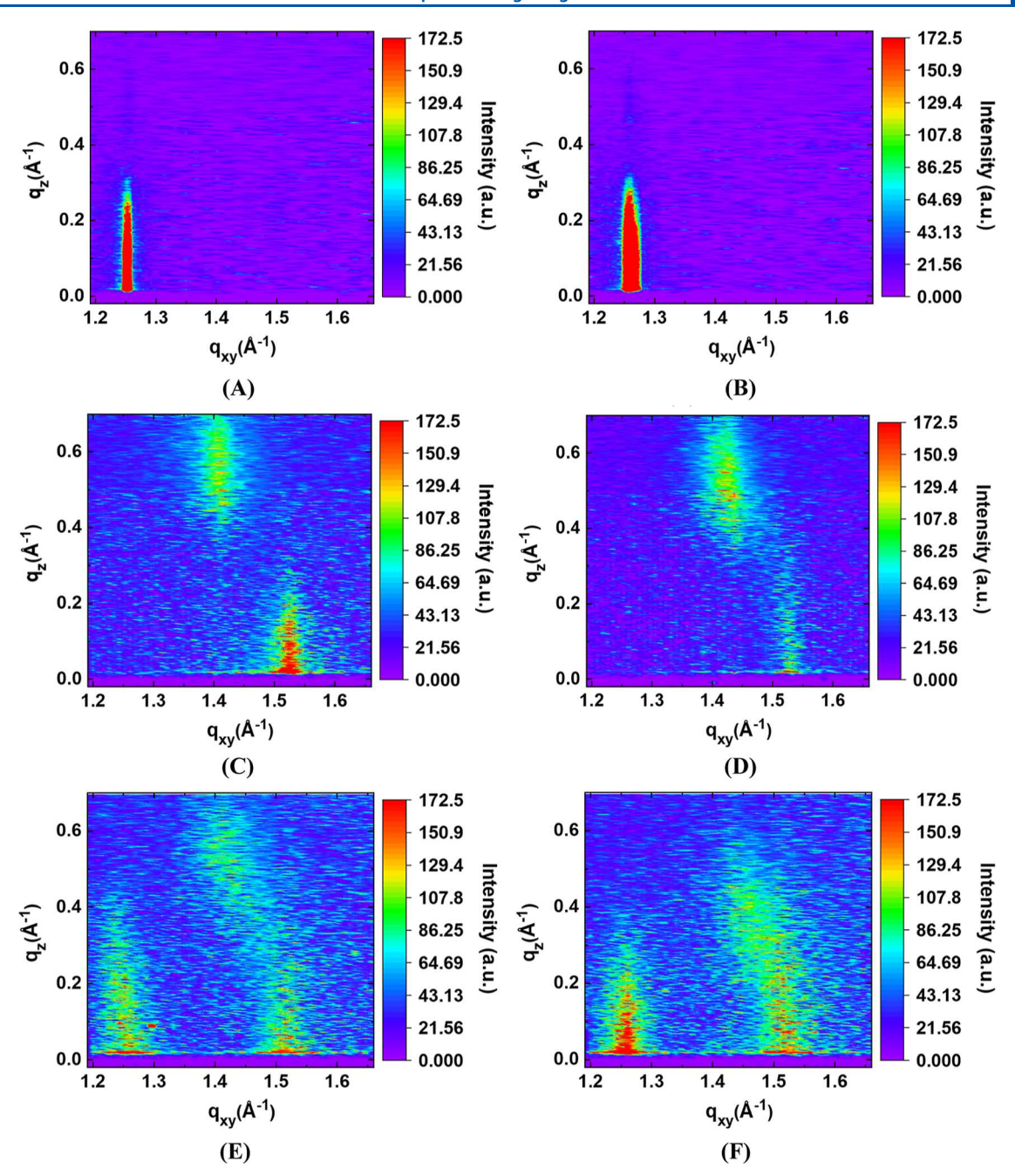


Figure 7. GIXD contour plots for pure PF monolayer at (A) $\pi \approx 10$ (B) 30 mN·m⁻¹; for C_{18} -0- C_{18} monolayer at (C) 10 (D) 30 mN·m⁻¹ and χ_{PF} = 0.50 mixed monolayer at (E) 10 mN·m⁻¹ and (F) 30 mN·m⁻¹.

the out of plane C_{18} -0- C_{18} peak, which was found at a slightly lower q_z than in the pure film and was beginning to merge with the in-plane Bragg peak; this is normally observed at higher film compression in pure C_{18} -0- C_{18} films (e.g., closer to the phase transition). While there might be slight differences in the nominal measured surface pressures between experiments, the mixed $\chi_{PF}=0.50$ film is more compact than a pure C_{18} -0- C_{18} film at the same surface pressure; as seen in the isotherms from Figure 1, the mixed films need to be compressed to significantly smaller mean molecular area in order to achieve the same surface pressure, and thus the diffraction pattern for the mixed film reflects this greater compression. We also cannot rule out the possibility of trace amounts of PF in the C_{18} -0- C_{18} rich regions of the film causing slight perturbations to the film structure. Notwithstanding, the overall X-ray results support

the occurrence of phase separation, in agreement with the cumulative measurements discussed above.

CONCLUSIONS

Phase separation occurs in mixed PF- C_{18} -0- C_{18} monolayers, with the main molecular-level contributions to this effect being the net repulsive interaction of perfluorinated and hydrogenated tail chains as well as the compact nature of both types of surfactant headgroups, which pack into stable crystalline lattices. Several intriguing questions arise from this work, which relate back to the structure of the "gemini without a linker" family of compounds. First, as the dominant intermolecular interaction in the mixed systems is the net repulsive interaction between fluorinated and hydrogenated tail chains, is it possible that the degree of miscibility in the films

might be further controlled by changing the gemini tail length relative to the perfluorocarbon tail length (Δ_{H-F} ; see⁷)? Dispersion interactions between fluorinated and hydrogenated surfactant tails will act to offset the "phobic" interaction and, thus, enable a degree of tunability in the interaction. This effect has been exploited to control phase separation and resulting film structure in simple fatty acid systems and as the behavior of the C_{18} -0- C_{18} geminis appears to be similar to that of fatty acids, similar control is plausible. An additional question is why the unique polygonal domain structures that have been reported in other perfluorinated surfactant-containing monolayers (see^{6,7,31} for example) are not present in the mixed gemini systems, despite the ability of both components to pack into crystalline films. This remains an elusive question and one that will be explored in more detail, and we posit that there are some subtle chemical structure requirements for the hydrogenated component in order to generate the polygonal domains. Systematic investigations of chemical structuremonolayer morphology relationships in the gemini surfactant family will be conducted to address this ongoing question.

ASSOCIATED CONTENT

Supporting Information

The Supporting Information is available free of charge at https://pubs.acs.org/doi/10.1021/acs.langmuir.3c02452.

Information includes: compressibility modulus plots, isotherms for pure and mixed films of PO and C_{18} -0- C_{18} , surface potential values, fitting results for relaxation curves, summary of XR measurements and numerical values from GIXD data for pure and mixed films of PF and C_{18} -0- C_{18} (PDF)

AUTHOR INFORMATION

Corresponding Author

Matthew F. Paige — Department of Chemistry, University of Saskatchewan, Saskatoon, Saskatchewan S7N 5C9, Canada; orcid.org/0000-0002-5552-8123; Email: matthew.paige@usask.ca

Authors

Srikant Kumar Singh – Department of Chemistry, University of Saskatchewan, Saskatoon, Saskatchewan S7N 5C9, Canada; orcid.org/0000-0001-5678-4228

Wei Bu − NSF's ChemMatCARS, Pritzker School of Molecular Engineering, University of Chicago, Chicago, Illinois 60637, United States; orcid.org/0000-0002-9996-3733

Pan Sun − NSF's ChemMatCARS, Pritzker School of Molecular Engineering, University of Chicago, Chicago, Illinois 60637, United States; orcid.org/0000-0002-6128-8656

Complete contact information is available at: https://pubs.acs.org/10.1021/acs.langmuir.3c02452

Notes

The authors declare no competing financial interest.

ACKNOWLEDGMENTS

Financial support for this work has been provided by the Natural Sciences and Engineering Research Council, the Canadian Foundation for Innovation, and the University of Saskatchewan. NSF's ChemMatCARS, Sector 15 at the

Advanced Photon Source (APS), Argonne National Laboratory (ANL) is supported by the Divisions of Chemistry (CHE) and Materials Research (DMR), National Science Foundation, under grant number NSF/CHE- 1834750. This research used resources of the Advanced Photon Source, a U.S. Department of Energy (DOE) Office of Science user facility operated for the DOE Office of Science by Argonne National Laboratory under Contract No. DE-AC02-06CH11357.

REFERENCES

- (1) Sharma, R.; Kamal, A.; Abdinejad, M.; Mahajan, R. K.; Kraatz, H.-B. Advances in the Synthesis, Molecular Architectures and Potential Applications of Gemini Surfactants. *Adv. Colloid Interface Sci.* **2017**, 248, 35–68.
- (2) Villa, C.; Baldassari, S.; Martino, D. F. C.; Spinella, A.; Caponetti, E. Green Synthesis, Molecular Characterization and Associative Behavior of Some Gemini Surfactants without a Spacer Group. *Materials* **2013**, *6* (4), 1506–1519.
- (3) Singh, S. K.; Yeboah, A.; Bu, W.; Sun, P.; Paige, M. F. Physicochemical Properties of Monolayers of a Gemini Surfactant with a Minimal-Length Spacer. *Langmuir* **2022**, *38* (51), 16004–16013
- (4) Acharya, D. P.; Kunieda, H.; Shiba, Y.; Aratani, K. Phase and Rheological Behavior of Novel Gemini-Type Surfactant Systems. *J. Phys. Chem. B* **2004**, *108* (5), 1790–1797.
- (5) Acharya, D. P.; Gutiérrez, J. M.; Aramaki, K.; Aratani, K.; Kunieda, H. Interfacial Properties and Foam Stability Effect of Novel Gemini-Type Surfactants in Aqueous Solutions. *J. Colloid Interface Sci.* **2005**, 291 (1), 236–243.
- (6) Paige, M. F.; Eftaiha, A. F. Phase-Separated Surfactant Monolayers: Exploiting Immiscibility of Fluorocarbons and Hydrocarbons to Pattern Interfaces. *Adv. Colloid Interface Sci.* **2017**, 248, 129–146.
- (7) Yan, C.; Paige, M. F. Pattern Formation in Phase-Separated Langmuir and Langmuir Monolayer Films. *Langmuir* **2021**, *37* (28), 8357–8369.
- (8) Rehman, J.; Sowah-Kuma, D.; Stevens, A. L.; Bu, W.; Paige, M. F. Immiscible Anionic Gemini Surfactant-Perfluorinated Fatty Acid Langmuir Monolayer Films. *Langmuir* **2019**, 35 (32), 10551–10560.
- (9) Rehman, J.; Sowah-Kuma, D.; Stevens, A. L.; Bu, W.; Paige, M. F. Mixing Behavior in Binary Anionic Gemini Surfactant-Perfluorinated Fatty Acid Langmuir Monolayers. *Langmuir* **2017**, 33 (39), 10205–10215.
- (10) Sowah-Kuma, D.; Fransishyn, K. M.; Cayabyab, C.; Martynowycz, M. W.; Kuzmenko, I.; Paige, M. F. Molecular-Level Structure and Packing in Phase-Separated Arachidic Acid-Perfluorotetradecanoic Acid Monolayer Films. *Langmuir* **2018**, 34 (36), 10673–10683.
- (11) Shibata, O.; Yamamoto, S. K.; Lee, S.; Sugihara, G. Mixed Monolayer Properties of Tetradecanoic Acid Withn-Perfluorocarboxylic Acids with 10, 12, 14, 16, and 18 Carbon Atoms. *J. Colloid Interface Sci.* 1996, 184 (1), 201–208.
- (12) Rehman, J.; Sowah-Kuma, D.; Stevens, A. L.; Bu, W.; Paige, M. F. Immiscible Anionic Gemini Surfactant-Perfluorinated Fatty Acid Langmuir Monolayer Films. *Langmuir* **2019**, *35* (32), 10551–10560.
- (13) Gaines, G. L. Insoluble Monolayers At Liquid-Gas Interfaces; Interscience Publishers: New York, 1966.
- (14) Rose, P. L.; Harvey, N. G.; Arnett, E. M. Chirality and Molecular Recognition in Monolayers at the Air-Water Interface. In *Advances in Physical Organic Chemistry*; Bethell, D., Ed.; Academic Press, 1993; Vol. 28, pp 45–138.
- (15) Gopal, A.; Lee, K. Y. C. Headgroup Percolation and Collapse of Condensed Langmuir Monolayers. *J. Phys. Chem. B* **2006**, *110* (44), 22079–22087.
- (16) Albrecht, O.; Gruler, H.; Sackmann, E. Pressure-Composition Phase Diagrams of Cholesterol/Lecithin, Cholesterol/Phosphatidic Acid, and Lecithin/Phosphatidic Acid Mixed Monolayers: A

- Langmuir Film Balance Study. J. Colloid Interface Sci. 1981, 79 (2), 319-338.
- (17) Bringezu, F.; Ding, J.; Brezesinski, G.; Zasadzinski, J. A. Changes in Model Lung Surfactant Monolayers Induced by Palmitic Acid. *Langmuir* **2001**, *17* (15), 4641–4648.
- (18) Jacobs, D. J.; Thorpe, M. F. Generic Rigidity Percolation in Two Dimensions. *Phys. Rev. E: Stat. Phys., Plasmas, Fluids, Relat. Interdiscip. Top.* **1996**, *53* (4), 3682–3693.
- (19) Shibata, O.; Krafft, M. P. Mixed Langmuir Monolayers Made from Single-Chain Perfluoroalkylated Amphiphiles. *Langmuir* **2000**, 16 (26), 10281–10286.
- (20) Barton, S. W.; Goudot, A.; Bouloussa, O.; Rondelez, F.; Lin, B.; Novak, F.; Acero, A.; Rice, S. A. Structural Transitions in a Monolayer of Fluorinated Amphiphile Molecules. *J. Chem. Phys.* **1992**, *96* (2), 1343–1351.
- (21) Fukuto, M.; Yang, L.; Nykypanchuk, D.; Kuzmenko, I. Transmission X-Ray Scattering as a Probe for Complex Liquid-Surface Structures. *J. Synchrotron Radiat.* **2016**, 23 (2), 519–531.
- (22) Acero, A. A.; Li, M.; Lin, B.; Rice, S. A.; Goldmann, M.; Azouz, I. B.; Goudot, A.; Rondelez, F. Molecular Packing in Water Supported Monolayers of F(CF2)11COOH and F(CF2)10CH2COOH. *J. Chem. Phys.* **1993**, *99* (9), 7214–7220.
- (23) Jacquemain, D.; Wolf, S. G.; Leveiller, F.; Lahav, M.; Leiserowitz, L.; Deutsch, M.; Kjaer, K.; Als-Nielsen, J. Dynamics of Two-Dimensional Self-Aggregation: Pressure and pH-Induced Structural Changes in a Fluorocarbon Amphiphile at Liquid-Air Interfaces. An x-Ray Synchrotron Study. *J. Am. Chem. Soc.* **1990**, *112* (21), 7724–7736.
- (24) Brzozowska, A. M.; Duits, M. H. G.; Mugele, F. Stability of Stearic Acid Monolayers on Artificial Sea Water. *Colloids Surf., A* **2012**, 407, 38–48.
- (25) Lee, Y.-L.; Liu, K.-L. Relaxation Behaviors of Monolayers of Octadecylamine and Stearic Acid at the Air/Water Interface. *Langmuir* **2004**, *20* (8), 3180–3187.
- (26) Vollhardt, D. Nucleation in Monolayers. Adv. Colloid Interface Sci. 2006, 123–126, 173–188.
- (27) Viseu, M. I.; Gonçalves da Silva, A. M.; Costa, S. M. B. Reorganization and Desorption of Catanionic Monolayers. Kinetics of Π t and A t Relaxation. Langmuir **2001**, 17 (5), 1529–1537.
- (28) Siegel, S.; Hoenig, D.; Vollhardt, D.; Moebius, D. Direct Observation of Three-Dimensional Transformation of Insoluble Monolayers. *J. Phys. Chem.* **1992**, *96* (20), 8157–8160.
- (29) Rehman, J.; Araghi, H. Y.; He, A.; Paige, M. F. Morphology and Composition of Structured, Phase-Separated Behenic Acid-Perfluor-otetradecanoic Acid Monolayer Films. *Langmuir* **2016**, 32 (21), 5341–5349.
- (30) Qaqish, S. E.; Paige, M. F. Rippled Domain Formation in Phase-Separated Mixed Langmuir-Blodgett Films. *Langmuir* **2008**, 24 (12), 6146–6153.
- (31) Eftaiha, A. F.; Paige, M. F. Phase-Separation of Mixed Surfactant Monolayers: A Comparison of Film Morphology at the Solid-Air and Liquid-Air Interfaces. *J. Colloid Interface Sci.* **2012**, 380 (1), 105–112.
- (32) Qaqish, S. E.; Paige, M. F. Mechanistic Insight into Domain Formation and Growth in a Phase-Separated Langmuir-Blodgett Monolayer. *Langmuir* **2007**, 23 (20), 10088–10094.